Asymptotic model for shape resonance control of diatomics by intense non-resonant light

2015 New J. Phys. 17 045020

(http://iopscience.iop.org/1367-2630/17/4/045020)

New Journal of Physics
The open access journal at the forefront of physics

Deutsche Physikalische Gesellschaft DPG
IOP Institute of Physics

Published in partnership with: Deutsche Physikalische Gesellschaft and the Institute of Physics

OPEN ACCESS

RECEIVED
1 December 2014

REVISED
20 February 2015

ACCEPTED FOR PUBLICATION
19 March 2015

PUBLISHED
27 April 2015

PAPER

Asymptotic model for shape resonance control of diatomics by intense non-resonant light

Anne Crubellier[1,5], **Rosario González-Férez**[2,3], **Christiane P Koch**[4] **and Eliane Luc-Koenig**[1]

[1] Laboratoire Aimé Cotton, CNRS, Université Paris-Sud 11, ENS Cachan, Bâtiment 505, F-91405 Orsay Cedex, France
[2] Instituto Carlos I de Física Teórica y Computacional and Departamento de Física Atómica, Molecular y Nuclear, Universidad de Granada, E-18071 Granada, Spain
[3] The Hamburg Center for Ultrafast Imaging, University of Hamburg, Luruper Chaussee 149, D-22761 Hamburg, Germany
[4] Theoretische Physik, Universität Kassel, Heinrich-Plett-Str. 40, D-34132 Kassel, Germany
[5] Author to whom any correspondence should be addressed.

E-mail: anne.crubellier@u-psud.fr, rogonzal@ugr.es, christiane.koch@uni-kassel.de **and** eliane.luc@u-psud.fr

Keywords: elastic ultracold collisions, shape resonances, laser-modified scattering

Abstract

We derive a universal model for atom pairs interacting with non-resonant light via the polarizability anisotropy, based on the long range properties of the scattering. The corresponding dynamics can be obtained using a nodal line technique to solve the asymptotic Schrödinger equation. It consists of imposing physical boundary conditions at long range and vanishing the wavefunction at a position separating the inner zone and the asymptotic region. We show that nodal lines which depend on the intensity of the non-resonant light can satisfactorily account for the effect of the polarizability at short range. The approach allows to determine the resonance structure, energy, width, channel mixing and hybridization even for narrow resonances.

1. Introduction

Ultracold collisions have been a focus of AMO physics research for the last two decades. The keen interest in the subject is due to two main aspects—collisions at very low energy are highly non-classical, and they show universal behavior [1, 2]. The quantum nature of ultracold collisions implies that the dynamics are governed by tunneling and resonances. The latter are at the core of an unprecedented control over the scattering particles that was achieved experimentally [3]. At the same time, the universal behavior of ultracold collisions has given rise to a thourough understanding of the underlying dynamics. For example, quantum-defect theory can be employed to calculate atom–atom scattering properties and bound rovibrational levels close to threshold [4–6].

A theory based solely on the asymptotic properties of the interaction potential has proven useful also for the description of photoassociation [7], i.e., the light-assisted formation of molecules [1, 8]. In particular, the nodal line technique to solve the Schrödinger equation in the asymptotic approximation was employed to determine the scattering length [9, 10] and potential energy curves [11] in several diatomic molecules. The formalism was extended to shape resonances [12, 13], which occur when a scattering state becomes trapped behind the centrifugal barrier for partial waves with $\ell > 0$, with ℓ being the rotational quantum number. This extension has allowed to capture all essentials of shape resonances in terms of a single parameter, the s-wave scattering length which universally characterizes the long-range two-body interaction.

An important aspect of shape resonances is that they lead to an increased pair density at short interatomic separations [14] and are thus crucial for molecule formation at ultralow temperatures [3, 15]. However, due to the rotational excitation involved in generating the centrifugal barrier, the lowest energies at which shape resonances occur typically correspond to temperatures of a few milli-kelvin. The interaction of non-resonant light with the polarizability of the atom pair can be used to shift the positions of shape resonances to lower energies [16, 17]. If the resonance position is made to match the trap temperature, the photoassociation rates are predicted to go up by two to three orders of magnitude [17]. This control is of a universal character, independent of the frequency of the light and the energy level structure of the molecule (as long as the frequency remains far

from any molecular resonance). Interestingly, non-resonant light control should also enable magnetoassociation by creating new Feshbach resonances and by strongly enlarging their width [18]. A non-resonant field affects not only shape resonances but also bound rovibrational levels by shifting their energies and hybridizing their rotational motion [17, 19]. This leads to alignment of the wave functions along the field direction [20].

These manifold proposals for control using non-resonant light call for an extension of asymptotic models [12, 13] to account for the coupling with non-resonant light via the polarizability anisotropy. Such an approach is promising as long as the relevant physics occurs at large interatomic separations and in an energy region close to threshold. This is the case both for shape resonance control in photoassociation [17] or Feshbach resonance engineering [18]. The dependence of the polarizability on interatomic separation is then universal and depends only on the polarizabilities of the constituent atoms [21, 22]. Including the interaction with a non-resonant field in asymptotic models should allow for predicting the field intensity that is required to modify the position of a shape resonance by a desired amount without exact knowledge of the potential. This is the question that we address here.

We test the asymptotic model against exact results for the strontium dimer which has recently been the subject of intense research both experimentally [23–26] and theoretically [27, 28]. The interest in Sr_2 is motivated by prospects to study the variation of the electron to proton mass ratio [29] and has already resulted in the observation of unusual non-adiabatic effects [30, 31]. Strontium molecules consisting of even-isotope atoms, such as $^{88}Sr_2$ or $^{86}Sr^{88}Sr$, for which the nuclear spin is zero, cannot be formed by magnetoassociation using a Feshbach resonance. Photoassociation then presents a viable alternative and non-resonant light control of shape resonances is particularly promising in this case [17]. The amount of intensity that is required to achieve such control is expected to depend on the field-free scattering length. The scattering length is very small for $^{88}Sr_2$, and large for $^{86}Sr^{88}Sr$, allowing a comparison of the intensity dependence for the two limiting cases. All of these facts together make the strontium dimer a natural benchmark for our asymptotic model.

The paper is organized as follows: we briefly recall the model for a diatomic molecule interacting with non-resonant light in section 2. Introducing reduced units of length and energy, we derive in section 3.1 a universal asymptotic Hamiltonian for this interaction. The nodal line technique to solve the corresponding asymptotic Schrödinger equation is introduced in section 3.2, with the computational details summarized in appendix A. For the example of $^{88}Sr_2$, we compare the results obtained from the asymptotic model with the nodal technique to those obtained from diagonalization of the full Hamiltonian (section 4.1). The differences in field-dressed shape resonances for molecules with small and large scattering lengths are illustrated in section 4.2, for $^{88}Sr_2$ and $^{86}Sr^{88}Sr$ molecules. We conclude in section 5.

2. Interaction of a diatom with a non-resonant optical field

The internuclear Hamiltonian of an atom pair in its electronic ground state in the presence of a non-resonant laser field, assuming the Born–Oppenheimer approximation, is written in the molecule-fixed frame as

$$H = T_R + \frac{\mathbf{L}^2}{2\mu R^2} + V_g(R) - \frac{2\pi I}{c}\left(\Delta\alpha(R)\cos^2\theta + \alpha_\perp(R)\right). \quad (1)$$

In equation (1), T_R and $\mathbf{L}^2/2\mu R^2$ are the vibrational and rotational kinetic energies for the motion of the two nuclei with reduced mass μ, interacting at interatomic separation R through the potential $V_g(R)$. The last term of equation (1), where c denotes the speed of light, represents the interaction with non-resonant light of intensity I, linearly polarized along the space-fixed Z axis. θ denotes the polar angle between the molecular axis and the laser polarization. The molecular polarizability tensor is characterized by its perpendicular and parallel components $\alpha_\perp(R)$ and $\alpha_\parallel(R)$, determined with respect to the molecular axis, which give rise to the polarizability anisotropy, $\Delta\alpha(R) = \alpha_\parallel(R) - \alpha_\perp(R)$. Note that the tensor α, which has the dimension of a volume (cm^3 in cgs units), is related to the polarizability $\underline{\alpha}$ which is deduced from the induced dipole moment (expressed in SI units of $CV^{-1}\,m^2$) by $\underline{\alpha} = 4\pi\epsilon_0\alpha$ with ϵ_0 the vacuum polarizability. In equation (1), the frequency of the non-resonant light is assumed to be far detuned from any resonance which allows for using the static polarizabilities. A large effect of the non-resonant light is expected if the light–matter interaction strength is large compared to the rotational kinetic energy. This corresponds to small rotational constant, or large reduced mass, and to large atomic polarizabilities.

The long-range behavior of the R-dependent polarizability, valid at $R > R_d = (4\alpha_1\alpha_2)^{1/6}$, can be derived from the polarizabilities of the two constituent atoms, α_1 and α_2. In the electronic ground state, one obtains [21, 22]

$$\alpha_{\parallel}(R) \approx \alpha_1 + \alpha_2 + \frac{4\alpha_1\alpha_2}{R^3} + \frac{4\left(\alpha_1 + \alpha_2\right)\alpha_1\alpha_2}{R^6}, \tag{2a}$$

$$\alpha_{\perp}(R) \approx \alpha_1 + \alpha_2 - \frac{2\alpha_1\alpha_2}{R^3} + \frac{\left(\alpha_1 + \alpha_2\right)\alpha_1\alpha_2}{R^6}. \tag{2b}$$

This R-dependence needs to be connected to *ab initio* data at short range. If this data is not available for the molecule of interest, the parallel and perpendicular polarizability components can be approximated (as in the present paper) by keeping them constant for $R < R_C$, and employing equations 2 for $R > R_C > R_d$. The specific value of R_C is not important for weakly bound levels and low-energy scattering states as long as the inequality is fulfilled which avoids the divergence occurring in $\alpha_{\parallel}$ at R_d.

The non-resonant field introduces a mixing of different partial waves of the same parity such that ℓ is not a good quantum number. For a given diatom, the rovibrational levels and low-energy scattering states can be determined by solving the Schrödinger equation associated to the Hamiltonian (1). To this end, H is represented by a mapped grid for the radial part [32] and a basis set expansion in terms of the spherical harmonics $Y_{\ell,m}(\theta, \varphi)$ for the angular part [33], taking advantage of the magnetic quantum number m being conserved. We label the field-dressed states by the field-free quantum numbers ℓ, m and v, adding a tilde to indicate that they are labels not quantum numbers. For the bound states, the field-dressed levels $\tilde{v}$, $\tilde{\ell}$ are diabatically connected to the field-free quantum numbers even for very high intensities. For the sake of simplicity this study is restricted to states with $m = 0$.

3. Asymptotic model

We derive an asymptotic approximation to the Hamiltonian (1) by extending the nodal line asymptotic model of [13] to account for the interaction of the diatom with a non-resonant field. This is possible since the influence of the non-resonant field on low temperature scattering states and weakly bound levels is dominated by the long range part of the interaction, characterized by a $1/R^3$-behavior (see equation (2)) and since the resonances under study are sufficiently close to the threshold. This method yields an efficient approach to study near threshold properties, such as shape resonances, of a diatomic molecule subjected to an intense non-resonant field.

3.1. Universal asymptotic Schrödinger equation for a diatom interacting with a non-resonant field

To derive the asymptotic approximation, we consider the Schrödinger equation with $V_g(R)$ replaced by its leading order asymptotic term, $V_g(R) \approx -C_6/R^6$ describing the van der Waals interaction. For the interaction with the non-resonant field, we also account only for the leading order term which scales as $1/R^3$. In addition, the R-independent term in $\alpha_{\perp}(R)$, lowers the dissociation limit. It reduces to $E_0 = -\frac{4\pi}{c}\alpha_0 I$, where α_0 denotes the atomic polarizability. Taking advantage of m being conserved and considering only $m = 0$, the asymptotic 2D-Schrödinger equation reads

$$\left[-\frac{\hbar^2}{2\mu}\frac{\mathrm{d}^2}{\mathrm{d}R^2} - \frac{C_6}{R^6} + \frac{\hbar^2}{2\mu}\frac{\mathbf{L}^2}{R^2}\right]\psi(R, \theta, \varphi) - \frac{2\pi I}{c}\left[2\alpha_0 + \frac{2\alpha_0^2}{R^3}\left(3\cos^2\theta - 1\right)\right]\psi(R, \theta, \varphi) = E\psi(R, \theta, \varphi). \tag{3}$$

If the atoms are not identical, α_0^2 needs to be replaced by $\alpha_1\alpha_2$, and $2\alpha_0$ by $\alpha_1 + \alpha_2$, see equation (2). Equation (3) can be rescaled by introducing a dimensionless reduced length x, a reduced energy $\mathcal{E}$ (defined with respect to the field shifted dissociation limit E_0) and a reduced laser field intensity $\mathcal{I}$

$$R = \sigma x,$$
$$E - E_0 = \epsilon\mathcal{E},$$
$$I = \beta\mathcal{I}.$$

The unit conversion factors for length σ, energy ϵ and laser intensity β contain the information specific to the free atom pair:

$$\sigma = \left(\frac{2\mu C_6}{\hbar^2}\right)^{1/4}, \tag{4a}$$

$$\epsilon = \frac{\hbar^2}{2\mu\sigma^2}, \tag{4b}$$

$$\beta = \frac{c}{12\pi}\frac{\hbar^{3/2}C_6^{1/4}}{\alpha_0^2(2\mu)^{3/4}} = \frac{c\sigma^3\epsilon}{12\pi\alpha_0^2}. \tag{4c}$$

The unit conversion factor for time, $\hbar/\epsilon$, is obtained from that of energy. The unit conversion factor for intensity, β, is proportional to $C_6^{1/4}\alpha_0^{-2}$ (i.e., to $\alpha_0^{-3/2}$, according to the approximate London formula for the van der Waals coefficient C_6) and to $\mu^{-3/4}$, such that larger polarizability and larger reduced mass require less intensity I for achieving the same value of the reduced intensity $\mathcal{I}$.

Employing atomic units, that is Bohr radii a_0 for σ, Hartree for ϵ and a_0^3 for the atomic polarizability, and expressing the laser intensity I in GW cm^{-2}, the reduced intensity is given by

$$\mathcal{I} = 4.274177\ 10^{-8}\ \frac{\alpha_0^2 I}{\epsilon\sigma^3}, \tag{5}$$

whereas the shift of the dissociation limit in reduced units is equal to

$$\mathcal{E}_0 = \frac{E_0}{\epsilon} = -\frac{4\pi\alpha_0 I}{c\epsilon} = -1.424725\ 10^{-8}\ \frac{\alpha_0 I}{\epsilon}. \tag{6}$$

When the reduced energy is expressed in μK, the numerical factors are equal to 13496.717 for the reduced intensity and −4498.93 for the reduced threshold shift, respectively. The asymptotic Schrödinger equation in reduced units is given by

$$\left[-\frac{\mathrm{d}^2}{\mathrm{d}x^2} - \frac{1}{x^6} + \frac{\mathrm{L}^2}{x^2} - \mathcal{I}\frac{\cos^2\theta - 1/3}{x^3} - \mathcal{E}\right] f(x, \theta, \varphi) = 0. \tag{7}$$

This universal asymptotic Schrödinger equation is valid at sufficiently large distances where the potential is dominated by the $1/x^6$ term, i.e., for $x > x_{\mathrm{asym}} = (C_8/C_6)^{1/2}$.

The asymptotic model in reduced units predicts that a field-free shape resonance is solely determined by equation (7), i.e., by its rotational quantum number ℓ, and by boundary conditions at a distance, $x_{0\ell} > x_{\mathrm{asym}}$. The value of $x_{0\ell}$ is related to the value in reduced units of the s-wave scattering length of the molecule. In the presence of a non-resonant field, the resonance energy (in reduced units) depends, apart from the field-free scattering length, on both the reduced laser field intensity $\mathcal{I}$ and the field-free rotational quantum number ℓ.

To account for the presence of the interaction with the non-resonant light in equation (7), we introduce below a modification of the nodal line technique to solve the asymptotic Schödinger equation for $x > x_{\mathrm{asym}}$. To this end, we first expand the wave function in spherical harmonics, $Y_{\ell,m}(\theta, \varphi)$(setting $m = 0$)

$$f(x, \theta, \varphi) = \sum_{\ell} y_\ell(x)\, Y_{\ell,m=0}(\theta, \varphi), \tag{8}$$

introducing the radial functions $y_\ell(x)$ for the different coupled channels ℓ. Equation (7) is then replaced by a system of coupled equations which can be written in vectorial form

$$\frac{\mathrm{d}^2}{\mathrm{d}x^2}\mathbf{y}(x) + (\mathbf{M} + \mathcal{E}\,\mathbb{1})\mathbf{y}(x) = 0, \tag{9}$$

where the vector $\mathbf{y}(x)$ is the set of functions $y_\ell(x)$, $\mathbb{1}$ denotes the identity and $\mathbf{M}$ is the matrix of the operator $\frac{1}{x^6} - \frac{L^2}{x^2} + \mathcal{I}\frac{\cos^2\theta - 1/3}{x^3}$ represented in the basis of spherical harmonics with ℓ-values of the same parity. We restrict our considerations here to $m = 0$ and even ℓ values varying from 0 to various $\ell_{\max}$ so that the model consists of $n = \ell_{\max}/2 + 1$ channels $\ell = 0, 2, \ldots, 2(n-1)$. We denote by $\mathbf{y}^j(x)$ a particular solution of the asymptotic Schrödinger equation in the coupled channel model

$$\mathbf{y}^j(x) = \sum_{\ell\ \mathrm{even}=0}^{\ell_{\max}} y_\ell^j(x)\, Y_{\ell,m=0}(\cos\theta), \tag{10}$$

where $y_\ell^j(x)$ is the radial component of the jth solution in the ℓth channel.

3.2. Nodal line technique

The nodal line technique is a method to solve the Schrödinger equation in the asymptotic region, which is applicable to the near-threshold energy range. The disregarded inner region is dominated by the potential $V_g(R)$, cf equation (1), and gives rise to a nodal structure of the wavefunction which is almost independent of its energy and the other interaction terms in the Hamiltonian (1). Therefore the dependence of the node positions on energy $\mathcal{E}$, on the centrifugal term $\propto \ell(\ell+1)$, or on any other small term in the Hamiltonian, such as the coupling with the non-resonant light $\propto \mathcal{I}$, can be estimated in the WKB approximation by a Taylor expansion of the local de Broglie wavelength. To first order, it introduces small contributions to the node positions which vary linearly with $\mathcal{E}$, $\ell(\ell+1)$, and $\mathcal{I}$, respectively.

When using the nodal line technique, the solution of the coupled equations (9) is carried out only for the zone where the asymptotic Hamiltonian is valid. At large distance, physical boundary conditions are imposed, depending on the sign of $\mathcal{E}$. For $\mathcal{E} < 0$, the radial wave functions exponentially decay in all channels, quantifying the energy of bound levels. For $\mathcal{E} \geqslant 0$, regular and irregular Bessel functions characterize the asymptotic behavior. At small distance, on the frontier of the inner zone, we require the radial part of the physical wave function in each channel y_ℓ^j to vanish at a position $x_{0\ell}$ that is located on a ℓ-dependent straight line in the $(\mathcal{E}, x)$ plane, the so-called nodal line [9, 34].

Without non-resonant field, the following positions were used:

$$x_{0\ell} = x_{00} + A\mathcal{E} + B\ell(\ell+1), \tag{11}$$

where the parameters x_{00}, A and B are characteristic of the chosen atom pair. In particular, x_{00} corresponds to the position of a node of the threshold s-wave wave function and is related to the s-wave scattering length [7]. A takes the variation of the node position with energy in the wave function with $\ell = 0$ into account. B describes the shift in the node of the threshold wave functions induced by the centrifugal term for the various partial waves, $\ell > 0$. The parameters x_{00}, A and B are adjusted, if possible, to reproduce experimental data, such as the positions of bound levels or resonances close to threshold, and the s-wave scattering length. They can also be determined by studying the nodal structure of wave functions calculated in a single-channel model using a molecular potential, when available.

In the absence of either reliable potentials or experimental data, there is a rough, but universal estimate of the parameters A and B given by very simple analytical formulas which depend only on the s-wave scattering length, $A^G = -(x_{00})^7/8$ and $B^G = (x_{00})^5/4$ [13]. These laws are deduced from the universal model of [4] which consists in a $-1/x^6$ potential limited by an infinite repulsive wall at a distance $x_{0_G} \to 0$. The WKB approximation is used to evaluate, in the vicinity of the threshold and for a not too high value of ℓ, the shift of the node located at x_{00} that arises from the contribution of the kinetic $A\mathcal{E}$ and centrifugal $B\ell(\ell+1)$ energies in the range $x_{0_G} \leqslant x \leqslant x_{00}$ [34]. Although the model becomes less realistic as x_{00} decreases, the corresponding A^G and B^G values are comparable to the values ajusted to experimental data [9, 10].

In the presence of a laser field, as it will be shown below (see section 4.1), an intensity dependent term has to be added to the nodal lines

$$x_{0\ell} = x_{00} + A\mathcal{E} + B\ell(\ell+1) + C\mathcal{I}. \tag{12}$$

The new term, $C\mathcal{I}$, i.e., lowest order in $\mathcal{I}$, accounts for the contribution of the interaction with the non-resonant field at short range. With this modification it is possible to obtain the bound levels, the resonance profiles of the shape resonances as well as the scattering length of the field dressed molecule for any intensity. The $\mathcal{I}$-dependent term can be evaluated in the same way as A^G and B^G. It is even possible to use exactly the same description of the polarizability as in the full-potential calculations (see sections 2 and 4): using the diagonal term of equation (7) for $x > x_C = R_C/\sigma$, replacing $\cos^2\theta$ by its approximate ℓ-independent mean value 1/2, and keeping a constant polarizability for $x \leqslant x_C$, we obtain (in reduced units)

$$C^G = -x_{00}^4/12 + 3x_C^4/48. \tag{13}$$

In order to determine bound levels and resonances, the calculation is performed in two steps. First, equation (9) is solved numerically by inward integration starting from a large value x_∞, imposing only large x boundary conditions. For $\mathcal{E} < 0$, i.e., levels below threshold, this value has simply to be larger than the outer Condon point. For $\mathcal{E} \geqslant 0$, x_∞ is chosen in the x-domain where the diagonal elements of the matrix $\mathbf{M} + \mathcal{E}\mathbb{1}$ reach their asymptotic form, that is $[\mathcal{E} - \ell(\ell+1)/x^2]$ for $\mathcal{E} > 0$ and $[1/x^6 - \ell(\ell+1)/x^2]$ for $\mathcal{E} = 0$. One can then use analytical solutions as initial values for the inward integration of the radial functions $y_\ell^j(x)$ in each channel and construct a set of linearly independent solutions $\mathbf{y}^j$ with the correct asymptotic behavior. There are n such solutions for bound levels and Siegert states. Their asymptotic behavior corresponds to either an exponentially decreasing function or an outgoing complex wave function in a given channel and zero in all others. For $\mathcal{E} \geqslant 0$, there are $2n$ linearly independent solutions, with an asymptotic behavior given by either a regular or an irregular Bessel function in a given channel and zero in all others, see reference [33] for $\epsilon > 0$ and reference [35] for $\epsilon = 0$.

In a second step, we calculate the physical solutions $\mathbf{z}^k$. They are linear combinations of the particular solutions $\mathbf{y}^j$ previously calculated. The coefficients are determined by imposing the radial components in each channel to vanish at the corresponding node position $x_{0\ell}$. This short range condition leads to a quantization of energy for the bound levels and Siegert states, see appendices A.1 and A.3, respectively. It also allows to determine the scattering length in the presence of the non-resonant field [36].

The continuous, n-fold degenerate spectrum at an energy $\mathcal{E}$ is described by multichannel scattering theory [37–39]. The chosen asymptotic boundary conditions allow for a direct determination of the energy-dependent reaction matrix, $\mathbf{K}(\mathcal{E})$, from which the scattering matrix, $\mathbf{S}(\mathcal{E})$, and the time-delay matrix, $\mathbf{Q}(\mathcal{E})$, are easily deduced. The details are presented in appendix A. In particular, the $\mathbf{Q}$ matrix is well-adapted to analyze shape resonances, by studying the energy variation of its lowest eigenvalue $q_1(\mathcal{E})$ which corresponds to Lorentzian

Table 1. Scaling factors defining the reduced units, cf equation (4), for $^{88}Sr_2$ and $^{86}Sr^{88}Sr$, obtained for $C_6 = 3246.97$ a.u. and $\alpha_0 = 186.25\ a_0^3$.

	$\sigma(a_0)$	$\epsilon\,(\mu\,\mathrm{K})$	$\beta(\mathrm{GW\ cm^{-2}})$	$\hbar/\epsilon\,(\mathrm{ns})$
$^{88}Sr_2$	151.053	86.3653	0.635782	88.4409
$^{86}Sr^{88}Sr$	150.617	87.876	0.641319	86.9204

profiles, see appendix A.2 for details. The eigenvalues $\tan[\tau_j]$ of the **K** matrix allow for determining the eigenphase sum $\tau(\mathcal{E})$. The energy variation of the derivative of the eigenphase sum yields also a profile of the shape resonances. The resonances are also finally characterized by calculating the energy variation of either population or mean value of $1/x^2$ inside the rotational barrier, see appendix A.2 for details.

4. Shape resonances in strontium

We investigate here the shape resonances of two isotopomers of strontium, $^{88}Sr_2$ and $^{86}Sr^{88}Sr$. They have the largest natural abundances (68% and 16%) and no nuclear spin. The *s*-wave scattering lengths are $a_S = -2\ a_0$, or −0.013 in reduced units, for $^{88}Sr_2$ [40] and $a_S = 97.9 a_0$, or 0.664 in reduced units, for $^{86}Sr^{88}Sr$ [41] (see table 1 for the scaling factors). For close to zero scattering length, quantum defect theory predicts shape resonances with $\ell = 4,\ 8,\ 12,\ \ldots$ i.e., for the case of $^{88}Sr_2$, whereas for a large scattering length, i.e., for $^{86}Sr^{88}Sr$, shape resonances with $\ell = 2,\ 6,\ 10,\ \ldots$ are expected [12]. We first test the validity of the asymptotic model by comparing to solutions obtained with the full Hamiltonian (1) for $^{88}Sr_2$ and then compare the behavior of the shape resonances as a function of the non-resonant light intensity for the two isotopomers.

4.1. Validity of the asymptotic model: position, width and hybridization of shape resonances in $^{88}Sr_2$

To test the validity of the asymptotic model, we solve the asymptotic Schrödinger equation (7) and compare to results obtained with the full Hamiltonian (1) [17], using the ground state potential energy curve from [23], adjusted to yield the relevant scattering length. The polarizabilities are computed from equation (2) for $R > R_C = 10\ a_0$ with an atomic polarizability of $\alpha_0 = 186.25 a_0^3$ [42]; for $R \leqslant R_C$ the polarizabilities are taken to be constant. We first need to determine the nodal lines. To this end we use [13] which gives the energies and widths of shape resonances as a function of the position of a node at short range. Reversely, knowing the position of a field-free shape resonance, it is possible to find a node position $x_{0\ell}$ (in a chosen *x*-interval) that yields a resonance at this energy value. Starting from the positions of the field-free shape resonances $\ell = 4$, 8, 12 and 16 [17], we first test nodal lines of the type (11). Since the coefficient *A* in equation (11) plays a minor role, it is taken to be constant and equal to $A = A^G = -(x_{00})^7/8$, the value of the 'universal' model [13]. $B(\ell)$ is taken to be a polynomial of degree 3 in $\ell(\ell+1)$; x_{00} and $B(\ell)$ are determined by a fit to the field-free shape resonance positions (the degree of the polynomial is 3 to fit the 4 data points exactly). Note that this fit provides the correct value, $a = -2a_0$, of the field-free scattering length.

However, when using the ansatz (11) to determine, in addition to the field-free positions of the shape resonances, the slopes of their dependence on the non-resonant field, the result is disappointing: for the four resonances the slopes are smaller by a factor of approximately 1.75 compared to those obtained from the full Hamiltonian. This finding suggests that the contribution of the short-range part of the interaction with the non-resonant field (for $x < x_{0\ell}$) is non-negligible, rendering the use of field-independent nodal lines insufficient. Remarkably, the effect of the coupling at short range on the intensity dependence of the resonance positions can be simply compensated, at least roughly, by introducing a scaling factor in the field intensity.

The influence of the interaction with the non-resonant field at short range on the resonance positions can be fully accounted for in the asymptotic model by making the nodal lines intensity-dependent, cf equation (12). Assuming *A* to be constant, $A = A^G$, as above, x_{00} and $B(\ell)$, taken to be a polynomial of degree 4 in $\ell(\ell+1)$, are adjusted to reproduce exactly the nodes of the field-free wave functions with $\ell = 0,\ 4,\ 8,\ 12,\ 16$. As above, this fit provides the correct value, $a = -2a_0$, of the field-free scattering length. Additionally, *C*, taken to be a polynomial of degree 3 in $\ell(\ell+1)$, is adjusted to reproduce exactly the variation of the node positions for $\ell = 4,\ 8,\ 12,\ 16$ with intensity when $\mathcal{I}$ is increased from 0 to 1 reduced unit. To this end, the ℓ-wave function of the rovibrational level closest to threshold is obtained numerically for $\mathcal{I} = 0$ and $\mathcal{I} = 1$, employing the Fourier grid method to solve equation (1) in a single channel approximation. For $\mathcal{I} = 1$, the single channel calculation represents an approximation. It is, however, well justified by the very small ℓ mixing observed in a coupled channels calculation for $\mathcal{I} = 1$, corresponding to $I = 0.64\ \ \mathrm{GW\ cm^{-2}}$ for $^{88}Sr_2$. The variation of the node positions at threshold with $\ell(\ell+1)$ is shown in figure 1 for $\mathcal{I} = 0$. Also plotted are the node positions at threshold of the 'universal' model, i.e., $B(\ell) = B^G = x_{00}^5/4$, corresponding to the same value of x_{00}. They do not deviate much from the node positions obtained from the full potential, except for large ℓ values. The node

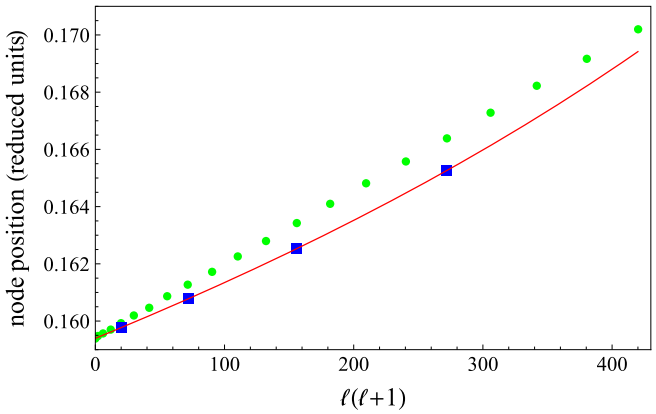

Figure 1. Nodal lines for $^{88}Sr_2$ in reduced units: the red line shows the variation of the node positions at threshold with $\ell\,(\ell+1)$ for $\mathcal{I}=0$, compared to the 'universal' model corresponding to the same value of x_{00} (green dots). The blue squares indicate the values for $\ell=4,\ 8,\ 12,\ 16$, adjusted to reproduce the field-free positions of the corresponding shape resonances [17]. The variation from $\mathcal{I}=0$ to $\mathcal{I}=1$ (in reduced units) of the nodes is too small to be visible in this figure.

positions in the presence of a weak non-resonant field, $\mathcal{I}=1$ in reduced units, differ from those for $\mathcal{I}=0$ by only about -0.5×10^{-4} reduced units, not visible on the scale of the figure. Adding this small and simple linear intensity dependence to the nodal lines yields spectacular agreement of the asymptotic model with the full Hamiltonian. This is demonstrated by the upper panel of figure 2 which compares the results of the asymptotic model with intensity-dependent nodal lines to those of the full Hamiltonian: almost no difference is visible on the scale of the figure. A linear intensity dependence of the nodal lines thus allows for utilizing the asymptotic model up to very large field intensities.

Note that all crossings between resonances or levels in figure 2 are in fact avoided crossings, and the diabatized lines are simply labeled by the $\tilde{\ell}$ value equal to the field-free ℓ value. Figure 2 also shows the behavior of the resonance width as a function of field intensity for the example of $\tilde{\ell}=8$ (lower panel). The calculations using the asymptotic nodal line technique were performed with 11 coupled channels, but we have checked for several values of $\tilde{\ell}$ and $\mathcal{I}$ that the positions of the shape resonances (up to $\tilde{\ell}=20$) do not change when $\ell_{\max}$ is increased (up to $\ell_{\max}=24$, corresponding to 13 coupled channels). The resonance positions and widths for $\tilde{\ell}=8,\ 12,\ 16$ shown in figure 2 have been obtained with the complex energy method, cf appendix A.3. For the resonance $\tilde{\ell}=4$, which is close to the top of the corresponding barrier at $\mathcal{I}=0$, the complex energy method does not apply and resonance profiles have been determined from the smallest eigenvalue of the time-delay matrix $Q(\mathcal{E})$, appendix A.2.

The intensity dependence of the resonance positions and widths shown in figure 2 is related to a strong hybridization of the rovibrational motion [16, 17]. The hybridization involves different aspects, which can be analyzed from profile calculations, cf appendix A.2. This is shown in figure 3, illustrating ℓ-mixing for the example of the $\tilde{\ell}=8$ resonance. The population density (per energy unit) trapped behind the centrifugal barrier (lower panel of figure 3) is essentially always concentrated in the $\ell=8$ channel. It increases rapidly when approaching the threshold. The crossing with the $\tilde{\ell}=12$ resonance does not visibly affect this evolution, whereas the crossing with $\tilde{\ell}=4$ involves a clear decrease of the population density in the $\ell=8$ channel (dip in the green line near 11 GW cm^{-2}). Note the different behavior of the percentages at short and long range. In the short-range region the population is essentially concentrated in the $\ell=8$ channel; and the short-range percentages converge exactly to the population percentages in the different channels of the corresponding $\tilde{\ell}=8$ bound level at threshold (middle panel of figure 3). In contrast, the asymptotic percentages (upper panel of figure 3) are very different from the short-range ones, with a very small contribution of the $\ell=8$ partial wave and large contributions of partial waves with $\ell=0$ and 2 at high intensities. The asymptotic percentages represent the partial wave decomposition of the continuum wave function associated to the lowest eigenvalue of the time delay matrix $Q(\mathcal{E})$. We stress here that this wave function is, inside the multiply degenerate continuum, the only wave function exhibiting resonant behavior. The behavior of the asymptotic percentages would probably be important if dynamical processes were considered.

4.2. Comparing $^{88}Sr_2$ and $^{86}Sr^{88}Sr$: intensity dependence of shape resonances in molecules with small and large scattering length

The crucial free parameter in the asymptotic model, and the only free parameter in the 'universal' asymptotic model, is the value of the *s*-wave scattering length (in reduced units) which determines the node positions. It is thus particularly instructive to compare the $^{88}Sr_2$ and $^{86}Sr^{88}Sr$ dimers. Since for small ℓ the differences between the 'universal' and the 'realistic' nodal lines are small, see figure 1, we use here 'universal' nodal lines (12) for

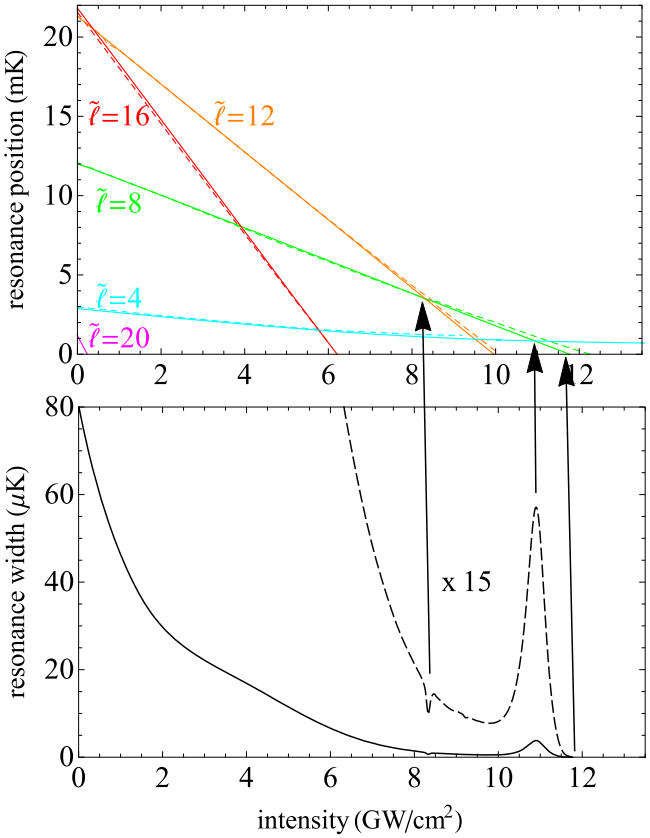

Figure 2. Upper panel: position of the shape resonances of $^{88}Sr_2$ as a function of non-resonant field intensity ($\tilde{\ell} = 4$ (cyan), $\tilde{\ell} = 8$ (green), $\tilde{\ell} = 12$ (orange), $\tilde{\ell} = 16$ (red) and $\tilde{\ell} = 20$ (magenta)), obtained from the asymptotic model with intensity-dependent nodal lines (solid lines) and the full Hamiltonian (dotted lines)—the results are almost indistinguishable. Lower panel: width of the $\tilde{\ell} = 8$ shape resonance of $^{88}Sr_2$ as a function of non-resonant field intensity. The dashed curve displays a 15-fold zoom of the solid one, showing the broadening (resp. narrowing) of the $\tilde{\ell} = 8$ resonance when it crosses the $\tilde{\ell} = 4$ (resp. $\tilde{\ell} = 12$) one, as indicated by the arrows. At threshold, also indicated by an arrow, the width tends to zero as expected.

$^{86}Sr^{88}Sr$, with coefficients $A = A^G$, $B = B^G$, $C = 0$ and the value of x_{00} determined by the s-wave scattering length. In this essentially explorative work, we have also limited the number of channels to 5 ($\ell_{max} = 8$), sufficient to study the $\tilde{\ell} = 2$ and $\tilde{\ell} = 6$ resonances.

Encouraged by the very good agreement between the asymptotic model and the full Hamiltonian for the shape resonances, we calculate for both isotopomers, in addition to the shape resonances, bound levels very close to threshold. Figure 4 displays the positions of shape resonances and bound levels for $^{88}Sr_2$, whereas the corresponding results for $^{86}Sr^{88}Sr$ are shown in figure 5. In both figures, we characterize each level or resonance by a value $\tilde{\ell}$, with the labeling done by continuity through avoided crossings ('diabatic' labeling) in two concording ways. First, we observe how the levels appear, as the number of channels in the calculations is enlarged; second, we analyze the channel decomposition for $\mathcal{I} = 0$. The intensity dependence of the resonance and bound level positions is extremely different for $^{88}Sr_2$ and $^{86}Sr^{88}Sr$: in figure 5, new $\tilde{\ell}$ values, $\tilde{\ell} = 2$ and $\tilde{\ell} = 6$, appear, all crossings are widely avoided and the $\tilde{\ell} = 6$ resonance crosses twice the threshold. It is worth mentioning that the theoretical energies obtained for the field-free bound $^{88}Sr_2$ levels with $\ell = 0$ and $\ell = 2$ (−74.64 reduced units or −134.4 MHz and −36.37 reduced units or −65.5 MHz) are in good agreement with the experimental values of −136.7 and −66.6 MHz for the $v = 62$, $\ell = 0$ and the $v = 62$, $\ell = 2$ shape resonances, respectively [24]. In the presence of the non-resonant field, the bound levels in figures 4 and 5 are of three types: (i)'pure' bound levels which are bound also in the field-free case; (ii) bound levels which appear when a shape resonance is pushed below threshold as the non-resonant field intensity is increased; and (iii)'supplementary' bound levels, which start tangentially to the threshold, i.e., regular scattering states that become bound as the field intensity is increased. The latter are due to a deepening of the $\tilde{\ell} = 0$ adiabatic potential as $\mathcal{I}$ increases. This effect is also observed for a very strong static electric field coupling to a permanent dipole moment [43].

Figure 6 analyzes the hybridization of a shape resonance for the example of the $\tilde{\ell} = 6$ resonance in $^{86}Sr^{88}Sr$. The features are similar to those shown in figure 3: in particular a drastic increase of the population density, especially in the $\ell = 6$ channel, is observed when the resonance comes close to the threshold. Simultaneously, there is almost no more contribution of the $\ell = 6$ partial wave in the asymptotic behavior.

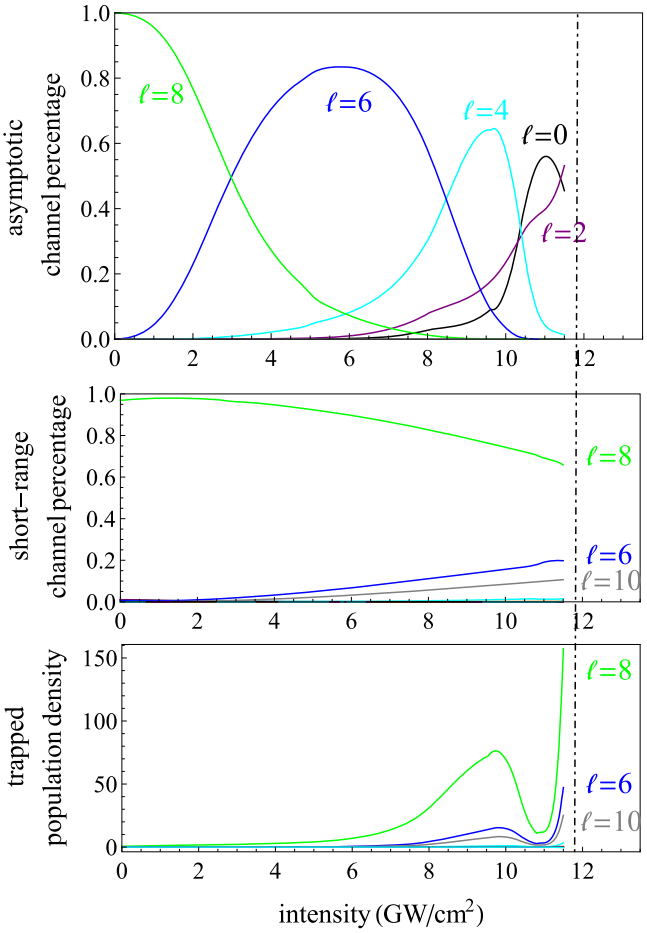

Figure 3. $^{88}Sr_2$: hybridization of the $\tilde{\ell} = 8$ shape resonance. The top panel shows the 'asymptotic' percentages in the different channels, i.e., the square of the partial wave components of the continuum wave function associated to the lowest eigenvalue of the time delay-matrix. The bottom panel displays the population densities (per energy unit) in the different channels which are trapped inside the corresponding rotational barriers; and the middle panel shows the 'short-range' channel percentages obtained from the population densities presented in the bottom panel. The dotted–dashed line indicates the crossing with threshold.

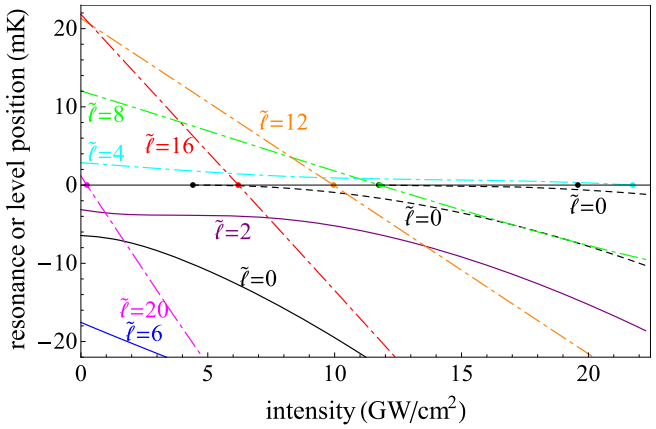

Figure 4. Positions of bound levels and shape resonances as a function of non-resonant field intensity for $^{88}Sr_2$, calculated with realistic, I-dependent, nodal lines (see text). Bound levels that are bound also in the field-free case are drawn as solid lines, dotted–dashed lines correspond to shape resonances which become bound at a certain intensity, and 'supplementary' levels, i.e., regular scattering states that become bound, are represented by dashed lines. The colors correspond to a 'diabatic' labeling.

5. Conclusions

We have generalized an asymptotic theory of diatomic scattering and weakly bound molecular levels [12, 13] to account for the interaction of the diatomic with non-resonant light through its polarizability anisotropy. Solving

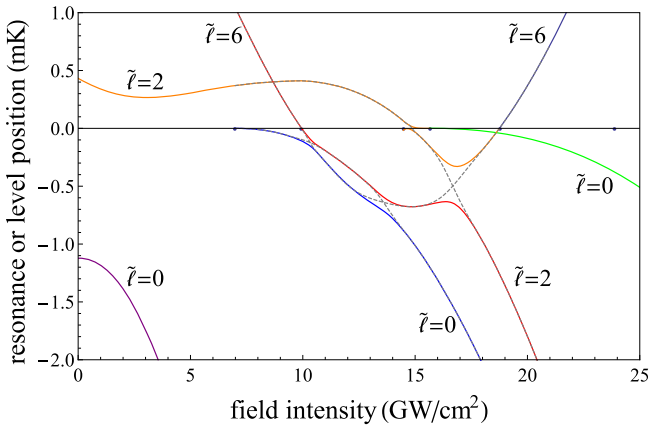

Figure 5. Positions of bound levels and shape resonances as a function of non-resonant field intensity for $^{86}Sr^{88}Sr$, calculated with 'universal' intensity-independent nodal lines. Avoided crossings are here clearly visible, making it impossible to match colors and labels. Diabatized curves, to which the labeling corresponds, are drawn in black dashed lines.

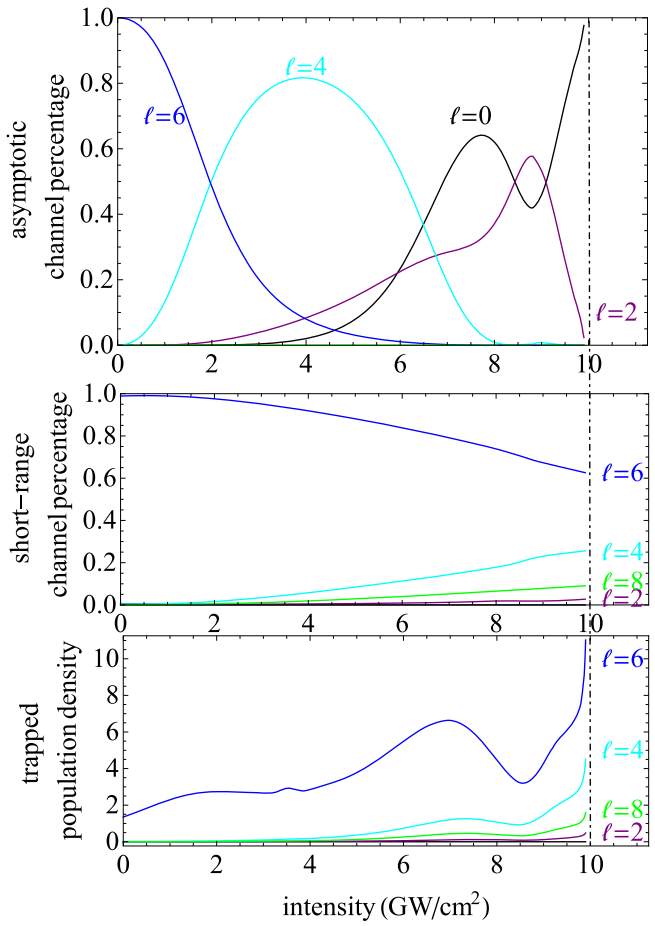

Figure 6. Hybridization of the $\tilde{\ell} = 6$ shape resonance of $^{86}Sr^{88}Sr$ as a function of non-resonant field intensity, analogously to figure 3. The dotted–dashed line indicates the crossing with threshold.

the asymptotic Schrödinger equation by a nodal line technique has allowed us to accurately reproduce the results of the full Hamiltonian for $^{88}Sr_2$ at all intensities. The agreement demonstrates the efficiency of the asymptotic model to predict the intensity dependence of the positions and widths of shape resonances. Moreover, due to the simplicity of the boundary conditions on the nodal lines, it is possible to utilize multichannel scattering theory and work with true continuum states. This allows for a detailed description of the resonance profiles which is accurate for broad and extremely narrow resonances alike.

The field-free scattering length is the essential parameter that determines the field-free position of shape resonances and also the position of the nodal lines. We have found an intensity dependence of the nodal line to be required to accurately account for the effect of the polarizability interaction at short range. Otherwise the slopes of the positions' intensity dependence in the asymptotic model differ by a factor of about 1.75 from those of the full Hamiltonian. A similar factor appears in a single channel approximation to the asymptotic model when intensity-independent nodal lines are considered [44]. The node positions are assumed to depend separately on energy, rotational quantum number and non-resonant field intensity. The channel mixing is thus completely ignored at short range.

The variation with field intensity of the resonance postions is found to be linear up to rather large field intensity. This suggests the use of perturbation theory based on field-free properties only, i.e., a single-channel model. A detailed discussion of such an approach will be presented in [44].

Our current approach allows for a universal prediction of the intensity dependence of shape resonances in arbitrary diatomic molecules, based solely on their scattering length, C_6 coefficient and reduced mass, and on the polarizability of the constituent atoms, without knowledge of the full interaction potential. This is important for utilizing non-resonant light control in molecule formation via photoassociation [17] or Feshbach resonances [18] as it allows to predict the required intensities. In addition to tuning the position and width of shape or Feshbach resonances, non-resonant light control can also be employed to change the background scattering length. This will be studied in detail elsewhere [36].

Acknowledgments

Laboratoire Aimé Cotton is 'Unité mixte UMR 9188 du CNRS, de l'Université Paris-Sud et de l'ENS Cachan', member of the 'Fédération Lumière Matière' (LUMAT, FR2764) and of the 'Institut Francilien de Recherche sur les Atomes Froids' (IFRAF). RGF gratefully acknowledges a Mildred Dresselhaus award from the excellence cluster 'The Hamburg Center for Ultrafast Imaging Structure, Dynamics and Control of Matter at the Atomic Scale' of the Deutsche Forschungsgemeinschaft and financial support by the Spanish Ministry of Science FIS2011-24540 (MICINN), grants P11-FQM-7276 and FQM-4643 (Junta de Andalucía), and by the Andalusian research group FQM-207.

Appendix A. Computational details

In the following we present the computational details of the nodal line technique applied to the asymptotic model for diatomics in a non-resonant field for the tasks of determining the energy and wave function of bound levels below the field shifted dissociation limit, and the energy profile and properties of shape resonances. All numerical calculations were performed using MATHEMATICA.

A.1. Bound levels

For a given value of energy, $\mathcal{E} = -k^2$, n linearly-independent solutions $\mathbf{y}^j$ are obtained by inward integration. Each solution j is related to a specific channel $\ell_j = 2(j-1)$ by imposing $y^j_\ell(x)$ to behave asymptotically as $y^j_\ell(x) \propto \exp(-kx)$ in the ℓ_j channel and zero in all others. The physical solution $\mathbf{z}$ is a linear combination,

$$\mathbf{z} = \sum_{j=1}^{n} a_j \mathbf{y}^j, \tag{A1}$$

where the radial component in each channel ℓ must vanish on the corresponding nodal line $x_{0\ell}$. The resulting linear system of n equations with n unknown variables a_j has a non-trivial solution if and only if

$$D_{\text{bound}}\left(\mathcal{E}\right) = \det\left(y^j_\ell\left(x_{0\ell}\right)\right) = 0, \tag{A2}$$

where $\det(\mathbf{M})$ is the determinant of the matrix $\mathbf{M}$. Equation (A2) is solved either by iteration on the energy $\mathcal{E}$ or by interpolation of $D_{\text{bound}}(\mathcal{E})$ on a set of $\mathcal{E}$-values and finding the corresponding zeros, $\mathcal{E}_{\text{bound}}$. Solution of the linear system of the n equations $\sum_{j=1}^{n} a_j\, y^j_\ell(x_{0\ell}) = 0$ corresponding to the n ℓ-values at an energy $\mathcal{E}_{\text{bound}}$ yields the coefficients a_j and thus the bound state wave functions of the various ℓ-channels. The coupled wave function $\mathbf{z}$ at the energy $\mathcal{E}_{\text{bound}}$ is normalized to one, such that hybridization can be measured by the weights $\varpi_\ell(\mathcal{E}_{\text{bound}}) = \int_{x_{0\ell}}^{x_\infty} [\sum_j a_j y^j_\ell(x)]^2\, \mathrm{d}x$.

A.2. Resonance profiles

To analyze the profiles of shape resonances in the n-fold degenerate continuous spectrum, we use multichannel scattering theory [37, 38]. For each energy $\mathcal{E}$, $\mathcal{E} = k^2 > 0$, we calculate $2n$ particular, linearly-independent, energy-normalized solutions of the Schrödinger equation (9) by inward integration. The initial conditions are taken at large distance x_∞, where the centrifugal term $1/x^2$ prevails. For each channel ℓ_j (where again $\ell_j = 2(j-1)$), we determine two particular solutions, denoted by $\mathbf{j}^j(x)$ and $\mathbf{y}^j(x)$, respectively, by imposing as asymptotic behavior in this channel either a regular $\sqrt{(k\pi x)/2}\,J_{\ell+1/2}(kx)$ or an irregular $\sqrt{(k\pi x)/2}\,Y_{\ell+1/2}(kx)$ energy-normalized Bessel function and zero in all other channels. The physical solutions of equation (9) are n linear combinations of the $2n$ calculated particular solutions which vanish on the nodal lines in each channel. Among all the possible sets of n particular combinations, we choose the 'standard' ones, $\mathbf{z}^j$, which asymptotically contain a regular component in the channel ℓ_j only

$$\mathbf{z}^j(x) = \sum_{j'=1}^{n}\Big[\ \delta_{j',j}\ \mathbf{j}^{j'}(x) + \ \mathbf{K}^j_{j'}\,\mathbf{y}^{j'}(x)\Big], \tag{A3}$$

where $\mathbf{K}$ is the so-called reaction matrix [37, 38]. Introducing two $n \times n$ matrices

$$\left(\mathbf{M}_{\rm reg}\right)^j_\ell = j^j_\ell(x_{0\ell}), \tag{A4a}$$

$$\left(\mathbf{M}_{\rm irreg}\right)^j_\ell = y^j_\ell(x_{0\ell}), \tag{A4b}$$

the conditions that the wave functions vanish on the nodal lines allow us to determine the $\mathbf{K}$- and $\mathbf{S}$- matrices [37, 38]

$$\mathbf{K} = -\left(\mathbf{M}_{\rm irreg}\right)^{-1}\cdot\mathbf{M}_{\rm reg}, \tag{A5}$$

$$\mathbf{S} = (1+\imath\mathbf{K})\cdot(1-\imath\mathbf{K})^{-1}. \tag{A6}$$

The existence and properties of a shape resonance can be determined by several different methods. An example of four different profiles that we have obtained in two particular cases (^{86}Sr^{88}Sr, $\tilde{\ell} = 2$, at a field intensity $\mathcal{I} = 5$ reduced units and ^{88}Sr$_2$, $\tilde{\ell} = 8$, at a field intensity $\mathcal{I} = 6.5$ reduced units) is displayed in figure A1.

The most suitable method for characterizing resonances is surely to study the time-delay matrix $\mathbf{Q}(\mathcal{E})$ [38, 39], which is related to the scattering matrix $\mathbf{S}$ by

$$\mathbf{Q} = -\imath\,\mathbf{S}^\dagger\ \cdot\ \frac{\mathrm{d}S}{\mathrm{d}\mathcal{E}}. \tag{A7}$$

When a narrow and isolated resonance shape resonance is present, the energy dependence of the lowest eigenvalue of $\mathbf{Q}$, $q_1(\mathcal{E})$ exhibits a Lorentzian profile

$$q_1(\mathcal{E}) \sim -\ \frac{\gamma_r}{\left(\mathcal{E}-\mathcal{E}_r\right)^2 + \left(\frac{1}{2}\gamma_r\right)^2}, \tag{A8}$$

where $\mathcal{E}_r$ is the resonance energy and γ_r its FWHM. The wavepacket associated to the corresponding eigenvector is resonantly delayed during its scattering by the attractive potential. This method can be extended to the analysis of overlapping resonances [47].

The lifetime $T = \hbar/\epsilon t$ of the resonance (in SI units) is calculated from the reduced lifetime $t = 1/\gamma_r$ and the reduced unit of time $\hbar/\epsilon$. The channel-mixing of the resonance can be characterized by the eigenvector corresponding to $q_1(\mathcal{E}_r)$, which gives the partial wave decomposition of the continuum wave function (one among the n wave functions of the n- multiple continuum) which concentrates the resonant character of the scattering at this intensity value.

The second method consists in diagonalizing the $\mathbf{K}$-matrix, with eigenvalues $\tan(\pi\tau_j)$. The corresponding eigenvectors can be used to construct the so-called 'eigenchannel wave functions', $\mathbf{u}^j$, wich have the same asymptotic behavior, $u^j(x) \propto J_{\ell+1/2}(kx) + \tan(\pi\tau_j)\,Y_{\ell+1/2}(kx)$, in all channels. The τ_j are called the eigenphase shifts. The total eigenphase shift

$$\tau(\mathcal{E}) = \sum_{j=1}^{n}\tau_j, \tag{A9}$$

increases by π when $\mathcal{E}$ passes through the resonance energy. The derivative with respect to the energy of the total eigenphase shift, $\tau'(\mathcal{E})$, exhibits a resonance profile, since it is related to the trace of the $\mathbf{Q}$ matrix by $\mathrm{Tr}\,[\mathbf{Q}(\mathcal{E})] = 2\tau'(\mathcal{E})$.

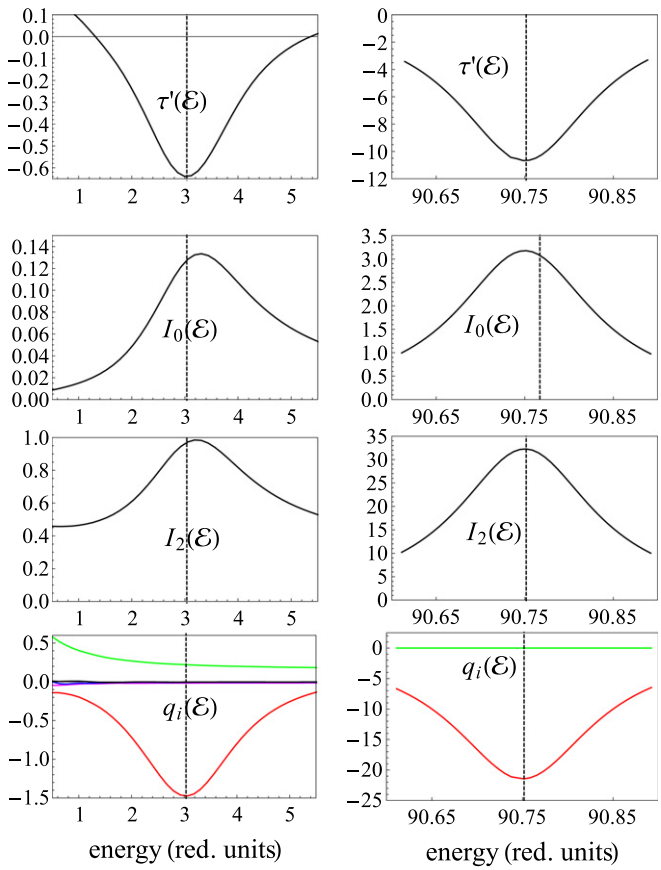

Figure A1. Comparison of four different methods allowing to characterize a shape resonance, in two particular cases: in the left column, a very broad resonance, $\tilde{\ell} = 2$ of $^{86}Sr^{88}Sr$, at a field intensity $\mathcal{I} = 5$ reduced units (calculated with 5 coupled channels), in the right one, a narrow resonance, $\tilde{\ell} = 8$ of $^{88}Sr_2$, at a field intensity $\mathcal{I} = 6.5$ reduced units (calculated with 11 channels). In each column are represented, from top to bottom, the energy variations of: the derivative with respect to energy $\tau'(\mathcal{E})$ of the sum of the eigenphases of the K-matrix, the total population density $I_0(\mathcal{E})$ trapped behind the centrifugal barriers, the mean value $I_2(\mathcal{E})$ of the operator $1/x^2$ and the eigenvalues $q_i(\mathcal{E})$ of the delay-matrix. One notices that all eigenvalues are zero (or positive) except the lowest one (in red), which exhibits a negative Lorentzian profile (indicating a positive time delay for the scattering). For a narrow resonance (right column) all profiles are quite similar. For a broad resonance (left column) the different methods yield slightly different profiles.

It is finally possible to characterize the profile of a shape resonance from the radial components $v_\ell^j(x)$ of any orthonormalized set of continuum wave functions. In practice, we have used energy-normalized wave functions associated to eigenvalues of the matrix $\mathbf{K}^T \cdot \mathbf{K}$. Introduction of the transposed matrix $\mathbf{K}^T$ allows one to eliminate numerical problems related to small asymmetries of the matrix $\mathbf{K}$. In addition, the scalar product of the standard functions $\mathbf{z}^j$ defined in equation (A3) is equal to $\mathbb{1} + \mathbf{K}^T \cdot \mathbf{K}$. Since a shape resonance is a metastable state in which two atoms are temporally kept close to each other, a resonance profile is also expected for the density (per energy unit) inside the barrier and for the expectation value of the $1/x^2$. Precisely we calculate the following integrals

$$I_p = \sum_{j=1}^{n} \sum_{\ell=1}^{n} \int_{x_{0\ell}}^{x_{\max}^{\ell}} \frac{\left[z_\ell^j(x)\right]^2}{x^p} \mathrm{d}x. \tag{A10}$$

With either $p = 0$ or $p = 2$; $x_{\max}^{\ell}$ is a very large value for $p = 2$; for $p = 0$, it is the position of the top of the centrifugal barrier $x_{\text{top}}^{\ell} = [\ell(\ell+1)/3]^{-1/4}$ for $\ell > 0$ and it is taken as $x_{\text{top}}^{\ell=2}$ for $\ell = 0$.

As shown in figure A1, the four calculated profiles, $q_1(\mathcal{E})$, $\tau'(\mathcal{E})$, $I_2(\mathcal{E})$ and $I_0(\mathcal{E})$, exhibit similar shape, especially for narrow resonances. In the latter case, the profiles $q_1(\mathcal{E})$ are perfectly given by equation (A8).

A.3. Resonances via the complex energy method

Shape resonances with large ℓ are very narrow, even for low field intensity. This is due to the presence of the broad and high potential barrier. Resonances lying very close to the field-shifted dissociation limit also have a very small width. It is quite difficult to detect narrow resonances and to calculate their characteristics from an analysis of the resonance profiles as described in appendix A.2. As an alternative, we therefore calculate the resonances as Siegert states with complex energy $\mathcal{E}_S = \mathcal{E} - \imath\gamma/2$ where the real and imaginary part are related to

the resonance energy and width [45, 46]. Siegert states are described by a complex wave function $\mathbf{z}$ whose asymptotic behavior corresponds to an outgoing wave in each channel.

To determine the Siegert states, we proceed similarly as for bound levels, cf appendix A.1. We first determine n linearly-independent particular complex solutions $\mathbf{y}^j$ of equation (9). Changing $\mathcal{E}$ into $\mathcal{E}_S = k^2$ results in a complex k-value. Inward integration, imposing an outgoing wave asymptotically in the ℓ_j channel and zero in all others yields the $\mathbf{y}^j$. The outgoing wave is written as a combination of the regular and irregular Bessel functions, $(-1)^{(\ell+1)/2}\sqrt{\pi x/2}\left[J_{\ell+1/2}(kx) + \imath Y_{\ell+1/2}(kx)\right]$. The physical Siegert wave function, obtained as a linear combination of the $\mathbf{y}^j$ solutions, has to satisfy the boundary condition at small x, i.e., the radial components in all channels have to vanish on the corresponding nodal line $x_{0\ell}$, calculated at the energy $\mathfrak{Re}(\mathcal{E}_S)$. These conditions are equivalent to a vanishing determinant $D_{\text{siegert}}(\mathcal{E}_S)$ of the radial ℓ-components of the n particular solutions $y_\ell^j(x)$ at the node positions. This condition quantifies the resonance energy to the value $\mathcal{E}_{S,r} = \mathcal{E}_r - \imath\gamma_r/2$.

References

[1] Weiner J, Bagnato V S, Zilio S and Julienne P S 1998 *Rev. Mod. Phys.* **71** 1
[2] Burnett K, Julienne P S, Lett P D, Tiesinga E and Williams C J 2002 *Nature* **416** 225
[3] Chin C, Grimm R, Julienne P and Tiesinga E 2010 *Rev. Mod. Phys.* **82** 1225
[4] Gao B 1998 *Phys. Rev.* A **58** 4222
[5] Gao B 2001 *Phys. Rev.* A **64** 010701
[6] Gao B 2003 *J. Phys. B: At. Mol. Opt. Phys.* **36** 2111
[7] Crubellier A and Luc-Koenig E 2006 *J. Phys. B: At. Mol. Opt. Phys.* **39** 1417
[8] Jones K M, Tiesinga E, Lett P D and Julienne P S 2006 *Rev. Mod. Phys.* **78** 483
[9] Crubellier A, Dulieu O, Masnou-Seeuws F, Elbs M, Knöckel H and Tiemann E 1999 *Eur. Phys. J.* D **6** 211
[10] Pasquiou B, Bismut G, Beaufils Q, Crubellier A, Maréchal E, Pedri P, Vernac L, Gorceix O and Laburthe-Tolra B 2010 *Phys. Rev.* A **81** 042716
[11] Vanhaecke N, Lisdat C, T'Jampens B, Comparat D, Crubellier A and Pillet P 2004 *Eur. Phys. J.* D **28** 351
[12] Gao B 2009 *Phys. Rev.* A **80** 012702
[13] Londoño B E, Mahecha J E, Luc-Koenig E and Crubellier A 2010 *Phys. Rev.* A **82** 012510
[14] Koch C P, Kosloff R, Luc-Koenig E, Masnou-Seeuws F and Crubellier A 2006 *J. Phys. B: At. Mol. Opt. Phys.* **39** S1017
[15] Boesten H M J M, Tsai C C, Verhaar B J and Heinzen D J 1996 *Phys. Rev. Lett.* **77** 5194
[16] Ağanoğlu R, Lemeshko M, Friedrich B, González-Férez R and Koch C P 2011 arXiv:1105.0761
[17] González-Férez R and Koch C P 2012 *Phys. Rev.* A **86** 063420
[18] Tomza M, González-Férez R, Koch C P and Moszynski R 2014 *Phys. Rev. Lett.* **112** 113201
[19] Tomza M, Skomorowski W, Musiał M, González-Férez R, Koch C P and Moszynski R 2013 *Mol. Phys.* **111** 1781
[20] Friedrich B and Herschbach D 1995 *Phys. Rev. Lett.* **74** 4623
[21] Heijmen T G A, Moszynski R, Wormer P E S and van der Avoird A 1996 *Mol. Phys.* **89** 81
[22] Jensen L, Åstrand P-O, Osted A, Kongsted J and Mikkelsen K V 2002 *J. Chem. Phys.* **116** 4001
[23] Stein A, Knöckel H and Tiemann E 2008 *Phys. Rev.* A **78** 042508
[24] de Escobar Y N M, Mickelson P G, Pellegrini P, Nagel S B, Traverso A, Yan M, Côté R and Killian T C 2008 *Phys. Rev.* A **78** 062708
[25] Stellmer S, Pasquiou B, Grimm R and Schreck F 2012 *Phys. Rev. Lett.* **109** 115302
[26] Reinaudi G, Osborn C B, McDonald M, Kotochigova S and Zelevinsky T 2012 *Phys. Rev. Lett.* **109** 115303
[27] Skomorowski W, Moszynski R and Koch C P 2012a *Phys. Rev.* A **85** 043414
[28] Skomorowski W, Pawłowski F, Koch C P and Moszynski R 2012b *J. Chem. Phys.* **136** 194306
[29] Zelevinsky T, Kotochigova S and Ye J 2008 *Phys. Rev. Lett.* **100** 043201
[30] McGuyer B H, Osborn C B, McDonald M, Reinaudi G, Skomorowski W, Moszynski R and Zelevinsky T 2013 *Phys. Rev. Lett.* **111** 243003
[31] McGuyer B H, McDonald M, Iwata G Z, Tarallo M G, Skomorowski W, Moszynski R and Zelevinsky T 2015 *Nat. Phys.* **11** 32
[32] Willner K, Dulieu O and Masnou-Seeuws F 2004 *J. Chem. Phys.* **120** 548
[33] Abramowitz M and Stegun I A 1964 *NBS Handbook of Mathematical Functions* (*Applied Mathematics Series 55*) (London: Harcourt Brace)
[34] Vanhaecke N 2003 *PhD Thesis* Université Paris XI, France
[35] Moritz M, Eltschka C and Friedrich H 2001 *Phys. Rev.* A **63** 042102
[36] Crubellier A, González-Férez R, Koch C P and Luc-Koenig E Controlling the scattering length with non-resonant light: predictions of an asymptotic model in preparation
[37] Seaton M J 1983 *Rep. Prog. Phys.* **46** 167
[38] Fano U and Rau A R P 1986 *Atomic Collisions and Spectra* (New York: Academic)
[39] Smith F T 1960 *Phys. Rev.* **118** 349
[40] Stein A, Knöckel H and Tiemann E 2010 *Eur. Phys. J.* D **57** 171
[41] Zhang J-C, Zhu Z-L, Liu Y-F and Sun J-F 2011 *Chin. Phys. Lett.* **28** 123401
[42] Lide D R (ed) 2009 *CRC Handbook of Chemistry and Physics* 91st edn (London: Taylor and Francis)
[43] González-Férez R and Schmelcher P 2009 *New J. Phys.* **11** 055013
[44] Crubellier A, González-Férez R, Koch C P and Luc-Koenig E 2015 Asymptotic model for shape resonance control of diatomics by intense non-resonant light: universality in the single-channel approximation *New J. Phys.* in press (arXiv:1412.7315)
[45] Siegert A J F 1939 *Phys. Rev.* **56** 750
[46] Simons J 1981 *Int. J. Quantum Chem.* **XX** 779
[47] Aiba K, Igarashi A and Shimamura I 2007 *J. Phys. B: At. Mol. Opt. Phys.* **40** F9